metals

MDPI

Article

Influence of Crystal Structure of Nitride Compound Layer on Torsion Fatigue Strength of Alloy Steel

Yoshitomi Yamada [1,*], Eto Hirohito [1] and Koji Takahashi [2]

[1] Vehicle Validation & Experiment Dept. No.2, Isuzu motor Ltd., Fujisawa-shi 252-0881, Japan; hirohito_etou@notes.isuzu.co.jp

[2] Faculty of Engineering, Yokohama National University, Kanagawa 240-8501, Japan; takahashi-koji-ph@ynu.ac.jp

* Correspondence: yoshitomi_yamada@notes.isuzu.co.jp; Tel.: +81-466-45-2045

Received: 7 November 2019; Accepted: 12 December 2019; Published: 16 December 2019

Abstract: The demand for high-strength components for commercial vehicles has recently increased. Conventional gas nitrocarburizing has been used to increase strength and productivity of the crankshaft. A potential-controlled nitriding process was recently developed to control the crystal structure of the nitride compound layer. It has been found that this treatment improves the bending fatigue strength compared with conventional treatment, and has the potential to cope with the increase in crankshaft strength. However, the effect of torsional fatigue strength has not been studied. Therefore, in this study, the influence of the crystal structure of the nitride compound layer on torsional fatigue strength was investigated. Two kinds of test specimens with different crystal structures of the compound layer were prepared using gas nitriding treatment with controlled nitriding potential for an alloy steel bar (JIS-SCM435). Torsional fatigue tests were carried out using these test specimens. Although the compound layer of these test specimens had different crystal structures, the hardness distribution and residual stress distribution on the diffusion layer were almost the same. The relationship between stress amplitude and number of cycles to failure (S-N curve) showed that the torsional fatigue limits of the specimens were almost the same. This indicates that the crystal structure of the nitride compound layer did not affect the torsional fatigue limits, because the origin of the torsional fatigue failure is inside the specimen.

Keywords: nitriding; torsional fatigue strength; potential-controlled nitriding process

1. Introduction

In commercial vehicles, increasing the strength of components is required to reduce the engine size and vehicle weight. Gas nitrocarburizing is a surface hardening technology similar to induction hardening and carburizing hardening, and is used to improve the strength and productivity of the crankshaft. By diffusing nitrogen from the surface of the components, a hard nitride compound layer forms on the outermost surface, and a diffusion layer forms on the inner side of the compound layer. Nitriding treatment is effective for improving the fatigue strength of parts because it can simultaneously increase the hardness and introduce compressive residual stress near the surface layer. Therefore, the influence of hardness and residual stress on the fatigue strength of surface treated metals have been reported in previous studies [1–3]. The influence of nitriding treatment on fatigue strength steels have been researched by several researchers [4–17]. Among them, the effects of diffusion layer depth [4–7], the conditions of gas nitrocarburizing [8], ion nitriding and gas nitriding [9] on fatigue strength were investigated. In addition, the fatigue behaviors of notched nitride steel were reported [10]. It was revealed that fatigue crack initiated sub-surface due to the stress gradient around the notch [10].

Furthermore, a combination treatment of nitriding and shot peening was investigated [11,12]. However, these studies did not consider the differences in the crystal structure of the nitride compound layer.

Recently, potential-controlled nitriding treatment has been developed by controlling the crystal structure of the nitride layer [13]. By controlling the nitrogen potential based on the Lehrer diagram [14], the crystal structure of the nitride compound layer can be changed from ε phase ($Fe_{2-3}N$) to γ′ phase (Fe_4N). It has been reported that fatigue strength under bending [15], tension–compression [16], and contact loading [17] was improved by inducing the γ′ phase. However, the effects of the differences in the crystal structures of nitride compound layer on torsional fatigue strength have not been studied. Therefore, it is unknown whether potential-controlled nitriding treatment contributes to the enhancement of torsional fatigue strength. The purpose of this study is to clarify the influence of different crystal structures of the nitride compound layer on the torsional fatigue strength of alloy steels. Two kinds of test specimens with different crystal structure of the compound layer were prepared using gas nitriding treatment with controlled nitriding potential for alloy steel. Torsional fatigue tests were carried out using these test specimens

2. Materials and Methods

The material used in this study was chromium molybdenum steel (JIS-SCM435). Table 1 shows the chemical composition of the material. Figure 1 shows a flowchart of the preparation of the test specimens. The specimens were quenched and tempered. After heat treatment, the specimens were machined to produce torsional fatigue test specimens. The torsional fatigue test specimen is an hourglass-type test specimen with a minimum diameter of 5 mm, as shown in Figure 2.

Table 1. Chemical composition of SCM435 (mass%).

	C	Si	Mn	P	S	Ni	Cr	Mo
SCM435	0.35	0.23	0.7	0.021	0.017	0.08	1.07	0.18

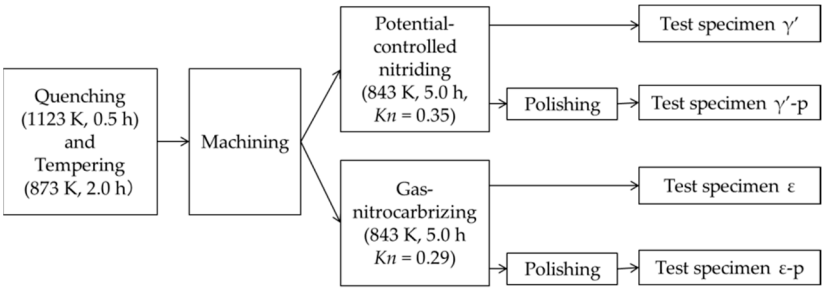

Figure 1. Flowchart of specimen preparation, four types of specimens were prepared.

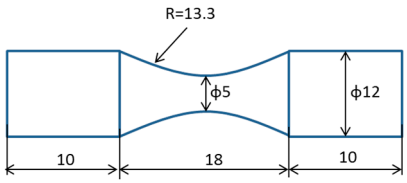

Figure 2. Shape of torsional fatigue test specimen, dimensions in mm.

2.1. Condition of Potential-Controlled Nitriding and Gas Nitrocarburizing

The potential-controlled nitriding and gas nitrocarburizing processes were carried out using an electric furnace (Onex Corporation., kanagawa, Japan), which can control the nitriding potential (*Kn*) by a hydrogen sensor. Two types of specimens, specimen γ′ and specimen ε, were prepared. In the potential-controlled nitriding process, *Kn* was set to 0.35, and in the gas nitrocarburizing

processes, *Kn* was set to 0.29 using a hydrogen sensor (SE-H2, STANGE Elektronik GmbH, Gummersbach, Germany).

2.2. Compound Layer Removal

In order to investigate the influence of the compound layer on the torsional fatigue strength, the compound layer was removed from some test specimens. These specimens were called γ′-p and ε-p, as shown in Figure 1. The compound layer was removed by repeated mechanical polishing and shape measurement to avoid significant changes in the shape. The depth of polishing was 15 μm in each specimen. The surface roughness of the test specimens with and without the compound layer was measured using a stylus-type surface-roughness-measuring instrument (SV-600, Mitutoyo Corporation, Tokyo, Japan).

2.3. Material Characterization of the Test Specimens

In-depth hardness distributions were measured at the minimum cross-section of the test specimen using a micro Vickers hardness tester (FM-300, Future-tech Corp., Kanagawa, Japan). The measurement was performed with a holding time of 10 s and an indenter load of 0.98 N.

The residual stress of the specimen was measured via the $\sin^2\psi$ method using a micro area X-ray residual stress measurement device (AutoMATE II, Rigaku Corp., Tokyo, Japan). Table 2 lists the measurement conditions. The in-depth residual stress distributions of the samples were measured by repeating electropolishing and measurement.

The structural observation was performed after mirror polishing the sample surface using an optical microscope and etching the sample with nital solution. It is well known that the crystal structures of γ′ phase (Fe_4N) and ε phase ($Fe_{2–3}N$) are face-centered cubic and hexagonal close packed structures, respectively [18]. Thus, the crystal structure of the compound layer was analyzed using electron backscatter diffraction (EBSD; NordlysNano, Oxford Instruments, oxford, UK).

Table 2. Detail of residual stress measurement conditions [19].

Method	ε-$Fe_{2–3}N$	γ′-Fe_4N	α-Fe
Characteristic X-ray		Cr-Kα	
Diffraction plane	(1,0,3)	(2,2,0)	(2,1,1)
Stress constant (MPa/deg)	−611	−611	−318

2.4. Fatigue Test Method

Torsional fatigue tests were performed with constant stress amplitude at a stress ratio $R = -1$ using a torsional fatigue testing machine (PBF-60, Tokyo Koki Co. Ltd., Tokyo, Japan). Fatigue tests were carried out at a frequency of 25 Hz. The fatigue limit was defined as the maximum value of the stress amplitude at which the specimen could endure 10^7 cycles of stress.

3. Results

3.1. Crystal Structure Identification of Compound Layer, Vickers Hardness, and Residual Stress at Surface Layer

Figure 3 shows the cross-sectional structure of each test specimen. The test specimens γ′ and ε had approximately 9 μm and 12 μm compound layers (white layer) formed on the surface, respectively. Figure 4 shows the phase analysis result of the compound layers of specimens γ′ and ε obtained using EBSD. In the compound layer of the test specimen γ′, the proportion of the γ′ phase was 70%, and the rest was ε phase. In contrast, in the compound layer of the test specimen ε, the proportion of the γ′ phase was almost 100%. The compound layer of γ′-p and ε-p specimens were removed completely by polishing. The arithmetic mean roughness (R_a) was 0.29 μm for specimen ε, 0.21 μm for specimen ε-p,

0.29 μm for specimen γ′, and 0.21 μm for specimen γ′-p. Thus, the difference in surface roughness was small.

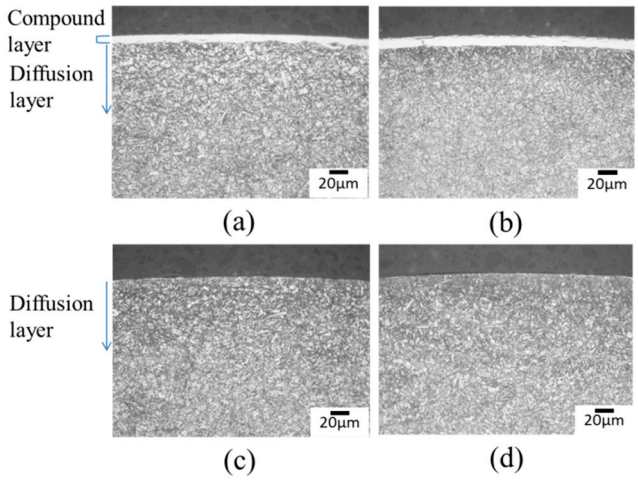

Figure 3. Microstructure of cross-section of each test specimen: (**a**) γ′; (**b**) ε; (**c**) γ′-p; and, (**d**) ε-p.

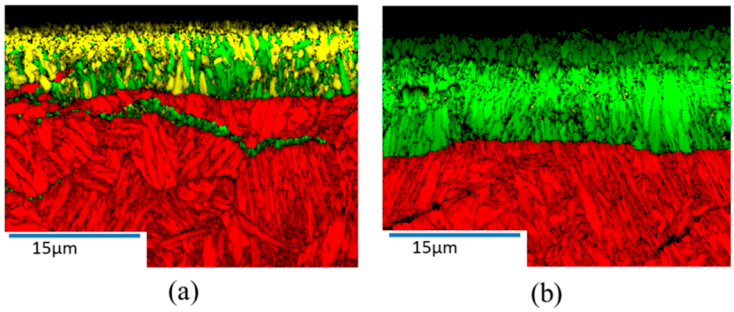

Figure 4. Crystal structure analysis of the test specimen: (**a**) γ′; (**b**) ε. Yellow color shows face-centered cubic (γ′ phase), green color shows hexagonal close packed structures (ε phase) and red color shows body-centered cubic (α phase).

Figure 5 shows the distributions of Vickers hardness. In test specimen γ′, the hardness at the compound layer was 724 HV, the maximum hardness at the diffusion layer was 600 HV, and the depth of the diffusion layer was 0.5 mm. In test specimen ε, the hardness at the compound layer was 790 HV, the maximum hardness at the diffusion layer was 570 HV, and the depth of the diffusion layer from the surface of the specimen was 0.5 mm. In specimens γ′-p and ε-p, the horizontal axis shows the depth from the surface after polishing. The hardness distributions at diffusion layer of test specimens γ′-p and ε-p were almost the same as those of the test specimens before the polishing.

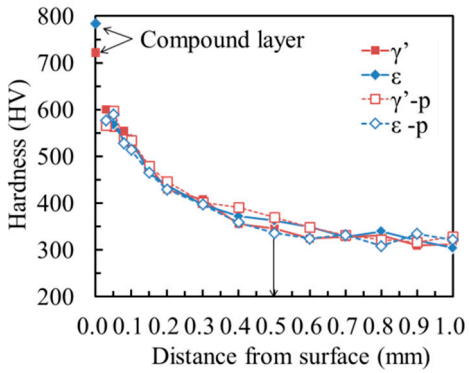

Figure 5. Vickers hardness of the compound and diffusion layers.

Figure 6 shows the measurement results of residual stress distribution. In specimens γ′-p and ε-p, the horizontal axis shows the depth from the surface after polishing. Table 3 lists the maximum compressive residual stress at the compound and diffusion layers of each test specimen. As the compound layer was removed in specimens γ′-p and ε-p, the residual stresses in the compound layer were not indicated. The maximum compressive residual stress at the diffusion layer was high in the specimens γ′-p and ε-p, as shown in Table 3. This additional compressive residual stress was introduced by mechanical polishing. However, the effect of the polishing on the depth was small. Thus, the effect of the additional compressive residual stress on the torsional fatigue strength was small. As the distance from the surface increased, the difference in residual stress between the specimens tended to decrease.

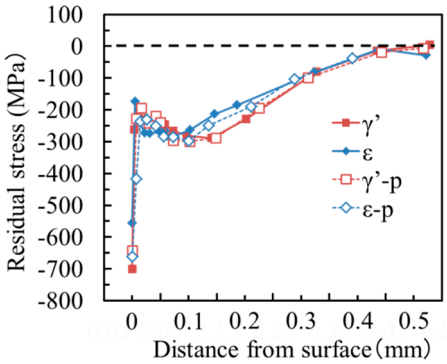

Figure 6. Residual stress distributions of each test specimen.

Table 3. Maximum compressive residual stress in each layer.

Specimen	Maximum Compressive Residual Stress (MPa)	
	Compound Layer	Diffusion Layer
γ′	701	288
ε	557	288
γ′-p	-	660
ε-p	-	641

3.2. Fatigue Test Results

S-N curves are shown in Figure 7. Comparison of the S-N curves of test specimens γ′ and ε show that the fatigue limits were equivalent. However, it was found that the fatigue life of specimens γ′ was longer than that of specimens ε. It was confirmed that fatigue life was shortened by polishing the compound layer, but there was no difference in the fatigue limit. These tendencies are consistent with the results of a rotating bending fatigue test using radical nitrided SNCM439 steel [20]. The reason why all the specimens show the same torsional fatigue limit is discussed in the next chapter.

3.3. Observation of Fatigue Cracks and Fractures

Figures 8 and 9 show surface cracks after the fatigue tests for N_f less than approximately 10^4 and more than 10^5 cycles, respectively. As shown in Figure 8, when N_f was approximately 10^4 cycles or less, the initial fatigue crack growth was in shear mode (Mode II), and after the cracks branched in the principal stress direction, they propagated in tensile mode (Mode I). Mode II cracks became longer when the compound layer was removed. As shown in Figure 9, when N_f was approximately 10^5 cycles or more, Mode II crack propagation was not observed, but Mode I fatigue cracks developed in the direction perpendicular to the principal stress from the beginning.

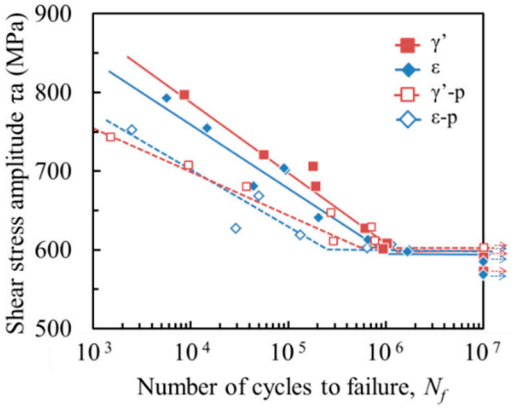

Figure 7. S–N curves of each test specimen.

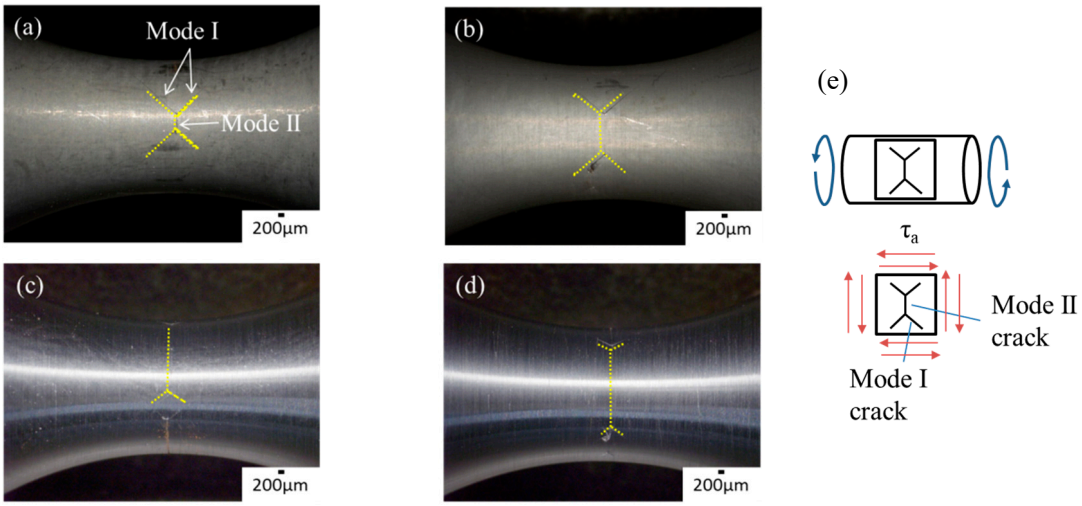

Figure 8. Surface crack shape of each test specimen (low cycle fatigue): (**a**) γ′ (τ_a = 796 MPa $N_f = 8.60 \times 10^3$); (**b**) ε (τ_a = 754 MPa $N_f = 1.48 \times 10^4$); (**c**) γ′-p (τ_a = 744 MPa $N_f = 1.50 \times 10^3$); (**d**) ε-p (τ_a = 753 MPa $N_f = 2.50 \times 10^3$); and, (**e**) image of applied stress and crack path.

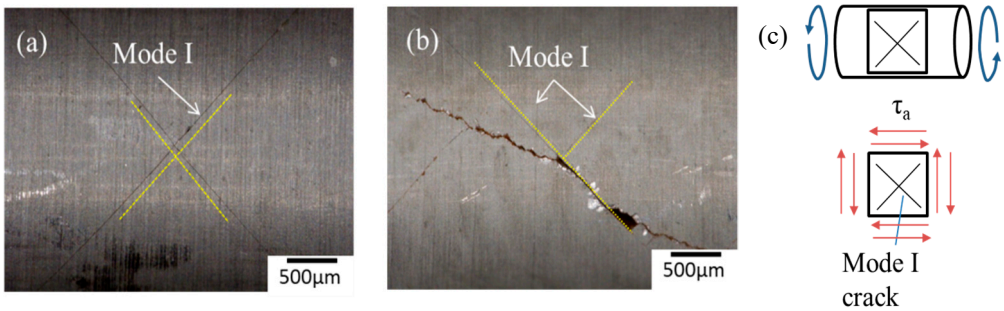

Figure 9. Surface crack shape of each test specimen (high cycle fatigue): (**a**) γ′ (τ_a = 680 MPa $N_f = 1.91 \times 10^5$); (**b**) ε (τ_a = 612 MPa $N_f = 6.61 \times 10^5$); and, (**c**) image of applied stress and crack path.

Figure 10 shows the observation results of the fracture surface of test specimen γ′, which fractured under a lower stress level near the fatigue limit. Fish-eye was observed on the fractured surface at a depth of approximately 0.35 mm from the surface. The crack initiation point of high cycle fatigue was inside the specimen. Thus, Mode II fatigue cracks were not observed in the specimens at N_f of approximately 10^5 cycles or more, as shown in Figure 8.

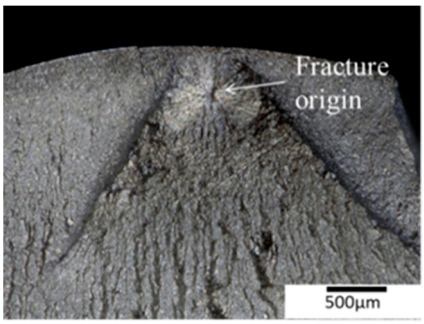

Figure 10. Fracture surface of γ′ test specimen (τ_a = 609 MPa $N_f = 1.03 \times 10^6$).

Figure 11 shows the relationship between the applied stress and Mode II crack length measured from the fracture surface. As the applied stress increased, the Mode II crack length tended to increase. In addition, a large difference was found in the Mode II crack length with the presence or absence of the compound layer. The propagation of Mode II cracks was suppressed by the compound layer. Therefore, the extension of the fatigue life in the high stress region was attributed to the presence of the compound layer.

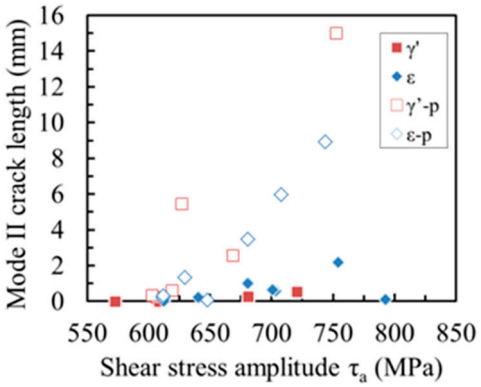

Figure 11. Relationship between Mode II crack length and applied stress.

4. Discussions

The results revealed that the torsional fatigue limit of nitrided steels did not depend on the type of nitride compound layer nor the presence or absence of the compound layer. This tendency differs from previous results of bending [15] and tension compression [16] fatigue tests. To discuss the differences in these results, we focused on the local torsional fatigue limit at each depth of the test specimens.

According to previous research, it was clarified that the torsional fatigue limit increased when compressive mean stress was applied in the axial direction [21]. Since compressive residual stress was induced by nitriding treatment in the test specimens used in this study, it was necessary to consider the influence of the compressive residual stress on the local torsional fatigue limit. Therefore, the local torsional fatigue limit was predicted based on the modified Goodman diagram by assuming that the residual stress is equivalent to the mean stress. The modified Goodman diagram is defined by Equation (1) [22]

$$\tau_w = \tau_{w0} - \frac{\tau_{w0}}{\sigma_B}\sigma_m \quad (1)$$

where τ_w is the local torsional fatigue limit under arbitrary mean stress (residual stress) σ_m, τ_{w0} is the torsional fatigue limit without mean stress, and σ_B is the tensile strength. Previous study [23] has shown that the torsional fatigue limit can be predicated by the following empirical equation (Equation (2)):

$$\tau_{w0} = 1.13\mathrm{HV} \quad (2)$$

The effective range of Equation (2) is HV < 400 [11], but in this study, it was applied to the case of HV up to approximately 800 HV. The relationship between τ_{w0} and σ_B was calculated using the following empirical Equation (3) [24]

$$\tau_{w0} = 0.35\sigma_B \quad (3)$$

By substituting Equations (2) and (3) to Equation (1), τ_w can be calculated by Equation (4)

$$\tau_w = 1.13\text{HV} - 0.35\sigma_m \quad (4)$$

Figure 12 shows the relationship between the distribution of τ_w calculated by Equation (4) for various test specimens and the applied stress distribution. The dotted straight line shows the applied stress distribution. The applied stress at the surface corresponded to τ_a = 609 MPa, where internal failure was observed (see Figure 10). Because of the characteristics of torsional stress, the distribution of applied stress decreased linearly with increasing distance from the surface. As can be seen in Figure 12, the intersection point of the predicated fatigue limit and the applied torsional stress distribution is not on the surface, but at a depth of approximately 0.2 mm from surface in all the test specimens. This is consistent with the experimental result shown in Figure 10. It is considered that the type and presence, or absence of the compound layer did not affect the fatigue limit, because the origin of fatigue crack near the fatigue limit was internal.

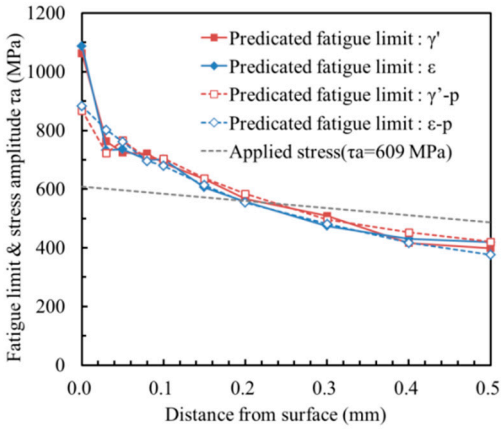

Figure 12. Distribution of predicated fatigue limits and applied stress of specimens.

On the other hand, in the case of bending and tension–compression fatigue tests, fatigue cracks originated from the surface of the specimens [15,16]. Thus, the differences in the crystal structure of the compound layer significantly affected the fatigue strength in the case of bending and tension–compression. However, the differences in the crystal structure of the compound layer had no effect on the torsion fatigue, because the crack initiation during torsion fatigue occurs below the compound layer.

5. Conclusions

In this study, the influence of crystal structure and presence of nitride compound layer on torsional fatigue strength were investigated. The results are summarized as follows:

(1) The crystal structure and presence of the nitride compound layer did not affect the torsional fatigue limit because the origin of the torsional fatigue failure is inside the specimen.
(2) It was found that the fatigue life is extended by changing the crystal structure of the compound layer from ε (HCP) to γ′ (FCC).
(3) The presence or absence of the compound layer affected the torsional fatigue life because the compound layer suppressed Mode II crack propagation.

(4) It was found that the failure origin can be estimated from the relationship between the predicted fatigue limit and applied stress distribution.

Author Contributions: Conceptualization, Y.Y. and E.H.; data curation, Y.Y.; investigation, Y.Y.; project administration, Y.Y. and E.H.; writing–original draft, Y.Y. and K.T.; writing–review & editing, K.T.

Funding: This research received no external funding.

Acknowledgments: The authors express our appreciation to Ito, Tsunenori., Onex Corp., for the potential controlled nitriding and gas nitrocarburizing treatment.

Conflicts of Interest: The authors declare no conflict of interest.

References

1. Sugimoto, K.I.; Hojo, T.; Mizuno, Y. torsional fatigue strength of newly developed case hardening TRIP-aided steel. *Metals* **2017**, *7*, 375. [CrossRef]
2. Sugimoto, K.; Mizuno, Y.; Hojo, T. Effects of vacuum-carburizing conditions on surface-hardened layer properties of transformation-induced plasticity-aided martensitic steel. *Metals* **2017**, *7*, 301. [CrossRef]
3. Xiaohui, Z.; Zhaoyi, S.; Desheng, X.; Yu, L. Local fatigue strength evaluation of shot peened 40Cr notched steel. *Metals* **2016**, *8*, 681.
4. Sirin, S.Y.; Sirin, K.; Kaluc, E. Effect of the ion nitriding surface hardening process on fatigue behavior of AISI 4340 steel. *Mater. Charact.* **2008**, *59*, 351–358. [CrossRef]
5. Alsaran, A.; Karakan, M.; Çelik, A. The investigation of mechanical properties of ion-nitrided AISI 5140 low-alloy steel. *Mater. Charact.* **2002**, *48*, 323–327. [CrossRef]
6. Genel, K.; Demirkol, M.; Çapa, M. Effect of ion nitriding on fatigue behaviour of AISI 4140 steel. *Mater. Sci. Eng. A* **2000**, *279*, 207–216. [CrossRef]
7. Çelik, A.; Karadeniz, S. Improvement of the fatigue strength of AISI 4140 steel by an ion nitriding process. *Surf. Coat. Technol.* **1995**, *72*, 169–173. [CrossRef]
8. Aoyama, S.; Ogawa, K. Rotating bending fatigue strength of Cr-Mo structural steel specimens carbonitrided at low temperature. *J. Soc. Mater. Sci. Jpn.* **1997**, *26*, 62–67. [CrossRef]
9. Ashrafizadeh, F. Influence of plasma and gas nitriding on fatigue resistance of plain carbon (Ck45) steel. *Surf. Coat. Technol.* **2003**, *174*, 1196–1200. [CrossRef]
10. Limodin, N.; Verreman, Y. Fatigue strength improvement of a 4140 steel by gas nitriding: Influence of notch severity. *Mater. Sci. Eng. A* **2006**, *435*, 460–467. [CrossRef]
11. Fernández Pariente, I.; Guagliano, M. About the role of residual stresses and surface work hardening on fatigue ΔKth of a nitrided and shot peened low-alloy steel. *Surf. Coat. Technol.* **2008**, *202*, 3072–3080. [CrossRef]
12. Croccolo, D.; Cristofolini, L.; Bandini, M.; Freddi, A. Fatigue strength of shot-peened nitrided steel: Optimization of process parameters by means of design of the experiment. *Fatigue Fract. Eng. M* **2002**, *25*, 695–707. [CrossRef]
13. Kawata, K. Gas Nitrocarburizing Furnace with Nitriding Potential Control System. *J. Jpn. Soc. Heat Treat.* **2009**, *49*, 64–68.
14. Lehrer, E. Über das Eisen Wasserstoff Ammoniak Gleichgewicht. *Z. Elektrochem.* **1930**, *36*, 383–392.
15. Hiraoka, Y.; Watanabe, Y.; Umezawa, O. Effect of Phase in surface compound layer on rotating bending fatigue strength for Gas-nitrided SCM435 steel. *Mater. Trans.* **2017**, *57*, 64–72.
16. Takagi, S.; Tonozuka, Y.; Nakamura, N.; Itou, T. Effect of crystal structure of surface compound layer on fatigue strength of nitrided SCM 435 steel. *Tetsu Hagane J. Iron Steel Inst. Jpn.* **2018**, *10*, 594–601. [CrossRef]
17. Kobayashi, A.; Maeda, S.; Imataka, H.; Gyotoku, Y.; Yuya, M.; Shimizu, Y.; Kanayama, M. Strengthening of low carbon alloy steel nitrided gear by generating γ′-Fe_4N phase. *Trans. Soc. Automov. Eng. Jpn.* **2014**, *45*, 1153–1158.
18. Dieter, L.; Ulrich, B.; Joachim, B.; Uwe, H.; Heinrich, K.; Wolfgang, L.; Heinz, -J.S. *Wärmebehandlung von Eisenwerkstoffen II: Nitrieren und Nitrocarburieren*, 5th ed.; Expert-Verlag Gmbh: Munich, Germany, 2009; pp. 11–12.
19. Tanaka, K.; Gu, Q.P.; Mikuriya, T.; Akiniwa, T. X-Ray residual stress measurement of gas-soft nitrided steel. *Trans. Jpn. Soc. Mech. Eng. Ser. A* **1996**, *62*, 2734–2740. [CrossRef]

20. Morino, K.; Kawagoishi, N.; Fukuda, K.; Wang, Q.; Kondo, E. Influence of compound layer on fatigue strength of radical nitrided SNCM439 steel. *Trans. Jpn. Soc. Mech. Eng. Ser. A* **2003**, *69*, 1490–1496. [CrossRef]
21. Zhang, W.; Akid, R. Mechanisms and fatigue performance of two steels in cyclic torsion with axial static tension/compression. *Fatigue Fract. Eng. Mater. Struct.* **1997**, *20*, 547–557. [CrossRef]
22. Wakita, M.; Kuno, T.; Hasegawa, T.; Sakurai, K.; Tanaka, T. Effect of shot peening on torsional fatigue strength of high strength spring steel and prediction of fatigue strength. *Trans. Jpn. Soc. Spr. Eng.* **2009**, *54*, 7–12.
23. Kanazawa, K.; Abe, T.; Nishizima, Y. *NIMS Material Data Base*; Date sheet No.9; National Research Institute for Metals: Tokyo, Japan, 1995.
24. Nakamura, H.; Horikawa, T. *Strength of Metal and Application of Fatigue Strength*, 2nd ed.; Corona Publishing: Tokyo, Japan, 2008; p. 44.